



# Ultrahigh purity plasma-enhanced atomic layer deposition and electrical properties of epitaxial scandium nitride

Running Title: PEALD of epitaxial ScN

Running Authors: Rayner, Jr. et al.

Gilbert B. Rayner, Jr.,<sup>1,a)</sup> Noel O'Toole,<sup>1</sup> Bangzhi Liu,<sup>2</sup> Jeffrey Shallenberger,<sup>2</sup> Jiadi Zhu<sup>3</sup>,  
Tomás Palacios<sup>3</sup>, Piush Behera<sup>4</sup>, Suraj Cheema,<sup>3,4,5</sup> Blaine Johs,<sup>6</sup> and Nicholas A. Strnad<sup>7</sup>

<sup>1</sup>The Kurt J. Lesker Company, 1925 PA-51, Jefferson Hills, PA 15025, USA.

<sup>2</sup>Materials Research Institute, The Pennsylvania State University, University Park, PA 16802, USA.

<sup>3</sup>Department of Electrical Engineering and Computer Science, Massachusetts Institute of Technology, 77  
Massachusetts Avenue, Cambridge, MA 02139, USA.

<sup>4</sup>Research Laboratory of Electronics, Massachusetts Institute of Technology, 77 Massachusetts Avenue,  
Cambridge, MA 02139, USA.

<sup>5</sup>Department of Materials Science and Engineering, Massachusetts Institute of Technology, 77  
Massachusetts Avenue, Cambridge, MA 02139, USA.

<sup>6</sup>Film Sense, 500 W South St #7, Lincoln, NE 68522, USA.

<sup>7</sup>Army Research Directorate, DEVCOM Army Research Laboratory, 2800 Powder Mill Road, Adelphi, MD  
20783, USA.

<sup>a)</sup>Electronic mail: [brucer@lesker.com](mailto:brucer@lesker.com)

Scandium nitride (ScN) by plasma-enhanced atomic layer deposition (PEALD) was demonstrated on silicon (100), sapphire (0001) and magnesium oxide (001) substrates under ultrahigh purity conditions using a new Sc precursor, bis(ethylcyclopentadienyl)scandium-chloride [ClSc(EtCp)<sub>2</sub>]. Out-of-plane x-ray diffraction patterns indicated single-crystal, cubic phase ScN deposited at 215°C on sapphire (0001) and magnesium oxide (001) substrates; phi-scans confirmed epitaxial growth. The ScN thin films grown on silicon with native oxide were polycrystalline with no preferential orientation. The ScN films showed a nitrogen-to-scandium ratio of approximately 1:1 measured by x-ray photoelectron spectroscopy, with ultra low levels of elemental impurities including 2.5 at.% chlorine, 0.9 at.% carbon and 0.4 at.% oxygen. ClSc(EtCp)<sub>2</sub> and N<sub>2</sub>-H<sub>2</sub> plasma were evaluated as a ScN co-precursors at substrate temperatures ranging from 200–300°C, where we identified an ALD window between 200–215°C. Images by field emission scanning electron

microscopy (FESEM) on 43 nm-thick films grown on untreated silicon revealed columnar grains with lateral sizes ranging from 16–28 nm. ScN conformality across 4:1 aspect ratio silicon trench structures with 312 nm-wide openings was also imaged by FESEM showing a top-to-bottom thickness ratio of 75%. ScN electrical properties were evaluated by performing Hall measurements to determine mobility, free electron concentration and resistivity. For ScN PEALD on magnesium oxide (001), the average mobility was 298 cm<sup>2</sup>/Vs with a carrier concentration of 2.88 x 10<sup>19</sup> cm<sup>-3</sup>. The average resistivity was 0.822 mΩ·cm.

## I. INTRODUCTION

ScN is a group 3, transition-metal nitride semiconductor that adopts a cubic rock salt crystal structure in its stable phase. Computational analysis of the electronic structure for intrinsic ScN has predicted an indirect band gap at 0.79–0.92 eV (Γ-X), as well as direct band gaps at 1.91–2.02 eV (X point) and 3.58–3.75 eV (Γ point).<sup>1-3</sup> Experimentally, the low energy direct band gap (X point), for nominally undoped epitaxial ScN with very low impurity levels, was measured at 2.06 eV.<sup>4</sup> The reported values in the literature, however, vary substantially between 2.06–3.1 eV,<sup>3-8</sup> where impurity levels have been shown to be a primary source of this variation.<sup>2,3,5</sup> ScN has received considerable attention for its potential use in thermoelectric applications,<sup>9-14</sup> and as an interlayer for epitaxial GaN growth.<sup>15-17</sup>

ScN is commercially relevant primarily because it forms a solid solution with aluminum nitride (AlN), resulting in aluminum scandium nitride (Al<sub>1-x</sub>Sc<sub>x</sub>N), which exhibits significantly enhanced effective coupling factor (K<sup>2</sup>) compared to undoped AlN and demonstrates ferroelectric switching at high electric fields.<sup>18,19</sup> The d<sub>33</sub> piezoelectric charge constant of Al<sub>1-x</sub>Sc<sub>x</sub>N increases with increased Sc content until x = 0.43, where larger concentrations of Sc cause phase segregation or formation of a metastable non-piezoelectric cubic phase.<sup>20</sup> Both AlN and Al<sub>1-x</sub>Sc<sub>x</sub>N have been

successfully integrated into bulk acoustic wave (BAW) devices, such as film bulk acoustic resonators (FBAR),<sup>21-23</sup> and derivative technology for radio frequency (RF) filters. Additional applications of  $\text{Al}_{1-x}\text{Sc}_x\text{N}$  include piezoelectric actuators for microelectromechanical systems (MEMS),<sup>24</sup> piezoelectric micromachined ultrasound transducers (PMUTs),<sup>25</sup> ferroelectric random-access memory (FeRAM),<sup>26</sup> and high operating temperature non-volatile memory (HOT-NVM).<sup>27</sup>

$\text{Al}_{1-x}\text{Sc}_x\text{N}$  thin films are traditionally deposited via reactive magnetron sputtering, which yields highly c-axis oriented columnar grains with sufficient process optimization and a compatible substrate.<sup>18-20</sup> However, sputtering is not suitable for coating high aspect ratio (HAR), vertically layered structures such as those desired for use in 3D embedded memory.<sup>28</sup> HAR structures may also be utilized in 3D piezoelectric MEMS (piezoMEMS) for emerging high-performance actuator applications.<sup>29</sup> Recently, there have been several reports of piezoelectric AlN grown by atomic layer deposition (ALD) that have shown promising crystalline quality and properties.<sup>30-32</sup> However, there are no reports of ALD  $\text{Al}_{1-x}\text{Sc}_x\text{N}$ , principally because there are no reported ALD processes for ScN. Various techniques have been employed to deposit ScN including reactive magnetron sputtering,<sup>3,5,6</sup> hybrid vapor phase epitaxy (HVPE),<sup>4</sup> and molecular beam epitaxy (MBE).<sup>7,8</sup> There are many challenges associated with growing ScN, especially the scarcity of commercially available Sc precursors suitable for nitrides, and the tendency of Sc to rapidly oxidize with exposure to oxygen.<sup>5,33</sup> Because ALD is not typically performed under ultrahigh vacuum (UHV), ultrahigh purity (UHP) conditions are therefore required to limit oxygen incorporation during ScN growth via ALD techniques.<sup>34</sup> In this report, we present a plasma-enhanced ALD (PEALD) process for growing cubic phase ScN under UHP conditions with oxygen content < 0.5 atom% using a new Sc precursor, bis(ethylcyclopentadienyl)scandium-chloride.

## II. EXPERIMENT

### A. ScN deposition

ScN PEALD was performed under UHP conditions in a Kurt J. Lesker Company (KJLC) ALD150LX perpendicular-flow reactor described elsewhere.<sup>34</sup> The Sc precursor used was bis(ethylcyclopentadienyl) scandium chloride [ClSc(EtCp)<sub>2</sub>] (Dockweiler Chemicals GmbH). This heteroleptic compound is a solid at room temperature, with a melting point at 95°C. ClSc(EtCp)<sub>2</sub> was contained in a stainless steel flow-through ampoule and kept at 180°C to develop adequate vapor pressure for delivery (vapor pressure  $\cong$  0.2 Torr, as determined experimentally by the precursor manufacturer). The process gases used were Ar, N<sub>2</sub> (99.999%, Airgas) and H<sub>2</sub> (99.999%, Linde). ScN films were grown by PEALD at substrate temperatures ranging from 200–300°C using ClSc(EtCp)<sub>2</sub> and a mixture of N<sub>2</sub> and H<sub>2</sub> (N<sub>2</sub>-H<sub>2</sub>) plasma species as co-precursors.

We define the ClSc(EtCp)<sub>2</sub> dose as the amount of time the associated ALD valves on the “in” and “out” sides of the flow-through ampoule were held open. During ClSc(EtCp)<sub>2</sub> dose and exposure steps, a downstream butterfly valve was used to limit conductance between the reactor and the pump, thereby increasing the pressure and Sc precursor residence time inside the reactor. N<sub>2</sub>-H<sub>2</sub> plasma was generated at ~0.3 Torr by a remote inductively coupled plasma (ICP) source operating at 13.56 MHz frequency and 600 W plasma power. The plasma gas flow rates were 40 sccm N<sub>2</sub> and 5 sccm H<sub>2</sub> (8:1). The reactor pressure was maintained at ~1 Torr during ClSc(EtCp)<sub>2</sub> and N<sub>2</sub>-H<sub>2</sub> plasma purge steps. ScN films were grown on silicon (Si), sapphire (Al<sub>2</sub>O<sub>3</sub>) and magnesium oxide (MgO) substrates; more specifically, as received 150 mm Si (100), 50 mm Al<sub>2</sub>O<sub>3</sub> (0001) and 1 cm x 1 cm MgO (001) substrates.

### B. Film characterization

## 1. Ellipsometry & XRR

ScN thickness and optical properties were determined *ex situ* by spectroscopic ellipsometry (SE) using a J. A. Woollam M-2000 spectroscopic ellipsometer over a range of wavelengths from 193–1000 nm. Ellipsometry measurements were also performed *in situ* during ScN growth using a Film Sense FS-8 multi-wavelength ellipsometer providing eight discrete wavelengths of ellipsometric data, distributed over a 370–950 nm spectral range. In both cases, a transparent Cauchy model, with no overlayer or surface roughness, was used to determine the ScN layer thickness and the refractive index. To avoid the effects of direct band gap absorption when modeling the ellipsometric data, the fitted data were limited to wavelengths  $\geq 526$  nm. To confirm the film thickness measured by ellipsometry, x-ray reflectivity (XRR) measurements were performed using a Malvern Panalytical X'Pert<sup>3</sup> MRD x-ray diffractometer with a Cu-K $\alpha$  source. Details about this instrument and the measurements performed are provided in the supplementary material.

## 2. XPS profiling

Film composition was measured by depth profile x-ray photoelectron spectroscopy (XPS) using a Physical Electronics VersaProbe III instrument equipped with a monochromatic Al K $\alpha$  x-ray source (1486.6 eV) and a concentric hemispherical analyzer. Quantification utilized instrumental relative sensitivity factors (RSFs) that account for the x-ray cross section and inelastic mean free path of the electrons. For the major elements (Sc, N), the  $1\sigma$  quantitative accuracy is expected to be within  $\pm 10$  rel%. Due to poor counting statistics, and finite background levels of C and O, the  $1\sigma$  accuracy is expected to be within  $\pm 20$ – $40$  rel% for the minor elements. Ion sputtering was accomplished using a 2 kV Ar<sup>+</sup> ion beam. Since detection of low levels of C and O were of interest, films were evacuated to  $< 2 \times 10^{-9}$  Torr prior to starting measurements. C and

O were acquired first in the depth profile to minimize any re-adsorption of C- and O-containing gases from the residual gases in the XPS chamber. This resulted in a lower limit of detection for both elements of ~0.1–0.2 at.%.

### 3. XRD

The structural phase of as deposited ScN was investigated by grazing incidence x-ray diffraction (GIXRD) using a Malvern Panalytical Empyrean diffractometer. Out-of-plane XRD and phi-scans were performed using Rigaku Smartlab and Malvern Panalytical Empyrean diffractometers, respectively. Details about these instruments and the measurements performed are provided in the supplementary material.

### 4. FESEM

To evaluate 3D conformality, Si trenches with a 1:4 aspect ratio were fabricated by deep reactive ion etching (RIE) and subsequently coated with ScN. The sample was then sectioned by both edge cleaving and focused ion beam milling (Thermo Scientific Scios 2 DualBeam), and finally imaged using a field emission scanning electron microscope (Zeiss Gemini 500). ScN deposited on planar Si was also imaged to investigate film morphology.

### 5. Hall probe

ScN electrical properties were investigated using the Van der Pauw method on 300 x 300  $\mu\text{m}$  ScN/ $\text{Al}_2\text{O}_3$  and ScN/MgO device areas. Contact pads consisted of a 50 nm Au layer on 20 nm Pd, which were fabricated at the four corners of each device. The Hall resistance was measured using 1 mA current and a magnetic field of  $\pm 2900$  Gauss, with the data demonstrating highly linear I-V behavior. A total of five devices were measured for each sample. The corresponding average values for ScN resistivity, mobility and carrier concentration are provided in Table II.

### III. RESULTS AND DISCUSSION

#### A. ScN Process Development

ScN films were measured in real-time during growth by *in situ* multi-wavelength ellipsometry (MWE) to assist in the development of the ScN PEALD process. The thickness and index of the evolving ScN film were determined using an ellipsometric model consisting of a Si substrate, native oxide layer and Cauchy-ScN layer. ScN growth-per-cycle (GPC) vs. ClSc(EtCp)<sub>2</sub> precursor dose time was investigated on untreated 150 mm Si (100) substrates to determine the dose saturation behavior of the PEALD process at substrate temperatures ranging from 200–300°C. For this investigation, the Sc precursor exposure and purge times remained fixed at 4 and 30 s; and the N<sub>2</sub>-H<sub>2</sub> plasma dose and purge times were fixed at 10 and 5 s, respectively. ClSc(EtCp)<sub>2</sub> purge time of 30 s ensured complete removal during purge steps. A description of the method used to generate this data is provided in the supplementary material.

ClSc(EtCp)<sub>2</sub> dose saturation curves are presented in Fig. 1(a), where each datapoint represents the average of three identical ScN depositions (error bars included). As observed in Fig. 1(a), the GPC saturates at ~0.15 Å/cycle with increasing ClSc(EtCp)<sub>2</sub> dose time at 200°C and 215°C. Similar saturation behavior is seen at 225°C with increasing ClSc(EtCp)<sub>2</sub> dose time, but the GPC is slightly higher. This behavior is also observed in Fig. 1(c), where the GPC at 215°C also shows a very slight increase compared to the GPC measured at 200°C. At substrate temperatures above 225°C, non-saturation becomes more evident with increasing dose time, along with more significant changes in the overall GPC with increasing substrate temperature as demonstrated in Figs. 1(a) and 1(c). As identified in Fig. 1(c), these results indicate that an ALD window exists between 200–215°C substrate temperature. At temperatures  $\geq 225^\circ\text{C}$ , the continued



This is the author's peer reviewed, accepted manuscript. However, the online version of record will be different from this version once it has been copyedited and typeset.  
PLEASE CITE THIS ARTICLE AS DOI: 10.1116/1.50004180

increase in GPC with  $\text{ClSc}(\text{EtCp})_2$  dose time and/or substrate temperature are indicative of pyrolysis of the Sc precursor.

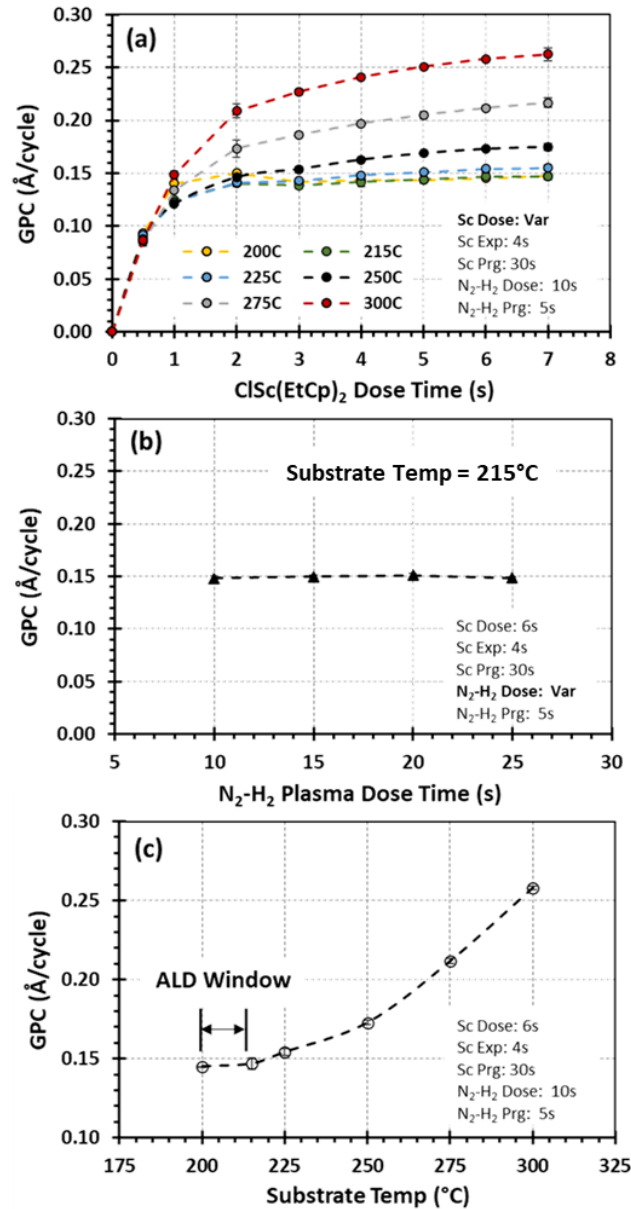


FIG. 1. ScN growth-per-cycle (GPC) vs. (a)  $\text{ClSc}(\text{EtCp})_2$  dose time at substrate temperatures ranging from 200–300°C and (b)  $\text{N}_2\text{-H}_2$  plasma dose time at 215°C substrate temperature. (c) ScN GPC vs. substrate temperature corresponding to a Sc precursor dose time of 6 s, where an ALD window is identified between 200–215°C.



The N<sub>2</sub>-H<sub>2</sub> plasma dose saturation curve presented in Fig. 1(b) shows no variation in the GPC between 10 and 25 s dose time, indicating that a 10 s plasma dose is sufficient to achieve saturation in the center of the reactor. SE measurements performed *ex situ*, however, revealed that ScN thickness uniformity across 150 mm Si substrates was improved by increasing the N<sub>2</sub>-H<sub>2</sub> plasma dose time (supplementary material, Fig. S2). Based on these results, a 20 s N<sub>2</sub>-H<sub>2</sub> plasma dose was utilized for all subsequent ScN depositions. The following process parameters were used to grow thicker PEALD ScN at 215°C for subsequent characterization: ClSc(EtCp)<sub>2</sub> dose = 6 s, ClSc(EtCp)<sub>2</sub> exposure = 4 s, ClSc(EtCp)<sub>2</sub> purge = 20 s, N<sub>2</sub>-H<sub>2</sub> plasma dose = 20 s and N<sub>2</sub>-H<sub>2</sub> plasma purge = 5 s (cycle time = 55 s). It is noted here that we observed some anomalous behavior of the ClSc(EtCp)<sub>2</sub> precursor after aging and thermal cycling. Details related to this behavior are included in the supplementary material and will be pursued for future study.

## B. Film Properties

For optical, compositional and structural analysis, ScN films were deposited on untreated 150 mm Si (100) substrates using the PEALD process parameters defined above. Nominal film thicknesses for x-ray characterization were 25 nm and 40 nm. The average SE thicknesses determined *ex situ* for ScN#1 (XPS sample) and ScN#2 (XRR, GIXRD sample) were 25.4 and 41.9 nm, respectively. A thicker film was deposited for GIXRD to improve the measurement signal-to-noise ratio. For both samples, the thickness non-uniformity (NU) was  $< \pm 4\%$  ( $1\sigma$ ) and the refractive index (at 633 nm wavelength) was 2.3 with NU  $< \pm 3\%$  ( $1\sigma$ ). The refractive index NU was primarily due to a higher value in the center vs. towards the outer diameter of the substrate. To confirm the measured SE thicknesses, XRR measurements were also performed at the substrate center and edge positions of ScN#2. The SE center and edge thicknesses were 40.6 and 42.3 nm;

and the XRR center and edge thicknesses were 39.7 and 41.8 nm, respectively. These results demonstrate good agreement between the two measurement techniques. XRR also revealed a slightly higher mass density at the center vs. edge positions as follows:  $\rho_{\text{ctr}} = 3.84 \text{ g/cm}^3$  and  $\rho_{\text{edge}} = 3.78 \text{ g/cm}^3$ . This difference in density could not be confirmed, however, due to the overlap between 95% confidence intervals for the center (3.78682, 3.90493) and edge (3.71889, 3.83265) positions. The density values reported here are lower than the reported bulk value of  $4.264 \text{ g/cm}^3$  for single-crystal, cubic phase ScN.<sup>35</sup>

A 5% increase in the refractive index was observed for ScN#2 at the center vs. edge positions, where  $n_{\text{ctr}} = 2.40$  and  $n_{\text{edge}} = 2.28$ . To better understand this increase, the optical properties were more thoroughly investigated *ex situ* by SE at the center and edge positions of both ScN#1 and ScN#2. A detailed description of the measurements and the corresponding analysis are provided in the supplementary material. An optical bandgap at  $\sim 2.45 \text{ eV}$  was determined for both films at the center and edge positions, which is in good agreement with reported values in the literature.<sup>3-8</sup> However, further work will be required to understand the observed changes in the ScN optical properties.

The XPS depth profile for ScN#1 is shown in Fig. 2, which contains the concentration vs. sputter depth of all major (Sc, N) and minor (Cl, C, O) components of the film. To determine the sputter depth, the SE thickness was used to convert sputter time to sputter depth. The high O and C impurity levels observed at the film surface are due to atmospheric exposure. As the  $\text{Ar}^+$  ions are used to sputter down into the bulk of the film, impurity levels decrease until a steady-state concentration is obtained. The native oxide interface is observed at  $\sim 24 \text{ nm}$ , and by  $30 \text{ nm}$  depth the bulk Si substrate is reached. Bulk concentrations for ScN were determined by averaging each elemental component between 7–17 nm sputter depth, as identified in Fig. 2. The bulk film

composition consists of  $48.8 \pm 0.5$  at.% Sc and  $47.3 \pm 0.4$  at.% N ( $N:Sc = 0.97 \pm 0.01$ ). Impurities are also present in the bulk of the film including  $2.3 \pm 0.2$  at.% Cl,  $0.9 \pm 0.3$  at.% C and  $0.4 \pm 0.2$  at.% O. The reported uncertainties represent the  $\pm 1\sigma$  variation associated with at.% averages over the specified range (i.e., 7–17 nm sputter depth).

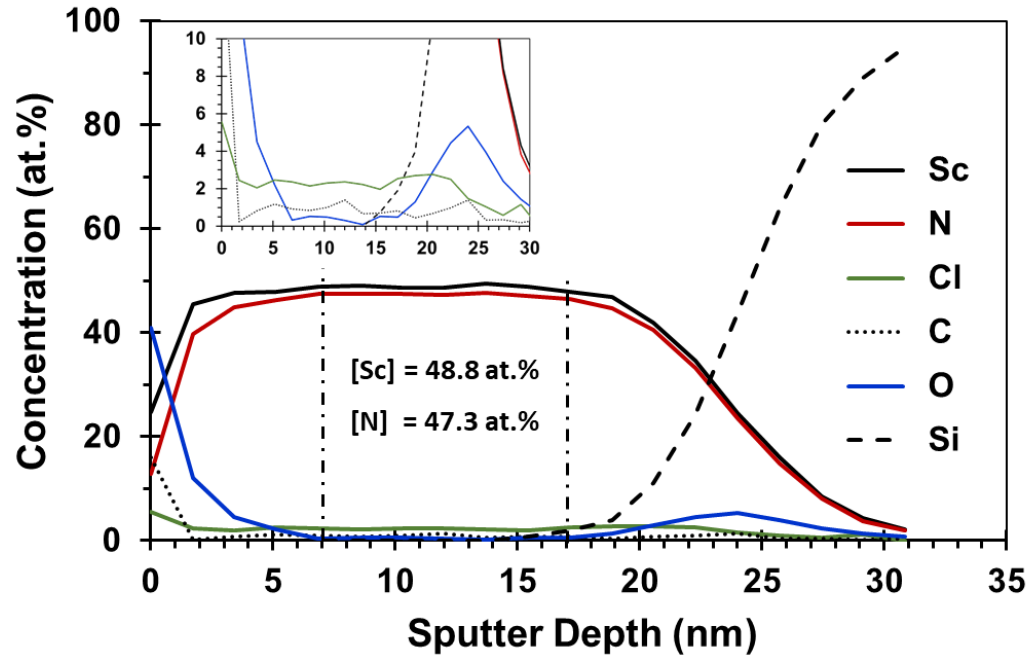


FIG. 2. XPS depth profile for ScN#1 showing the concentration vs. sputter depth of all major and minor elemental components of the film. Bulk concentrations were determined by averaging each component between 7–17 nm sputter time.

XPS was also performed on a sample taken from the edge of ScN#1, which showed a consistent composition with the substrate center as follows:  $48.4 \pm 0.4$  at.% Sc,  $47.4 \pm 0.4$  at.% N,  $2.6 \pm 0.1$  at.% Cl,  $0.9 \pm 0.2$  at.% C and  $0.3 \pm 0.2$  at.% O. The N-to-Sc ratio in this case is slightly higher ( $N:Sc = 0.98 \pm 0.01$ ), but within the estimated uncertainty. A summary of the XPS results are presented in Table I. At both center and edge positions, the bulk O content measured was just

above the detection limit of the instrument. When compared to other nitrides such as TiN, it has been shown that ScN films (grown by reactive magnetron sputtering techniques) are more highly susceptible to oxygen contamination.<sup>5</sup> To deposit ScN with high crystalline and electrical quality, it was concluded that UHV or other environments containing low amounts of oxygen are required. The results presented in Fig. 2 demonstrate that UHP conditions provide a suitable environment for the growth of ScN by PEALD techniques.<sup>34</sup>

TABLE I. Summary of XPS depth profile results for ScN film composition.

<i>Position</i>	<i>Sc (at.%)</i>	<i>N (at.%)</i>	<i>N:Sc</i>	<i>Cl (at.%)</i>	<i>C (at.%)</i>	<i>O (at.%)</i>
Center	48.8 ± 0.5	47.3 ± 0.4	0.97 ± 0.01	2.3 ± 0.2	0.9 ± 0.3	0.4 ± 0.2
Edge	48.4 ± 0.4	47.4 ± 0.4	0.98 ± 0.01	2.6 ± 0.1	0.9 ± 0.2	0.3 ± 0.2

The GIXRD patterns for ScN#2 presented in Fig. 3(a) show (111), (200), (220) and (311) reflections matching cubic phase ScN (PDF 04-001-1145). The narrow peak at ~52° and broad peak at ~55° are artifacts of the GIXRD method stemming from the Si substrate. These features can be eliminated and/or suppressed by rotating the substrate (supplementary material, Fig. S7). Similar GIXRD patterns are observed at the center and edge positions indicative of a uniform, polycrystalline, cubic phase structure across the 150 mm Si (100) substrate. ScN films were also deposited on Al<sub>2</sub>O<sub>3</sub> (0001) and MgO (001) substrates for further structural analysis.

For ScN grown on Al<sub>2</sub>O<sub>3</sub> (0001), the XRD pattern in Fig. 3(b) shows reflections consistent with a single preferred out-of-plane (111) orientation. The rocking curve FWHM taken at the (111) peak was measured to be 0.19° and is consistent with epitaxial growth. Since the Al<sub>2</sub>O<sub>3</sub> (0001) substrate is hexagonal, the ScN adopts a (111) out-of-plane orientation to ensure favorable epitaxial lattice matching between the three-fold symmetry of the cubic (111) plane and underlying rhombohedral lattice hexagonal ( $R\bar{3}c$ ) of Al<sub>2</sub>O<sub>3</sub>. Additionally, based on the ScN (111) and (222) peak position,  $a_0 = 4.53 \text{ \AA}$ , which is slightly larger than the expected bulk value. In-plane crystal orientation was determined using a phi-scan [supplementary material, Fig. S8(a)], which showed 6-fold symmetry due to the underlying hexagonal structure of the sapphire substrate and confirms epitaxial growth. The observed 6-fold symmetry for the ScN (131) reflections suggests the presence of twinned in-plane alignment common amongst cubic structures grown on Al<sub>2</sub>O<sub>3</sub>.

The XRD pattern for ScN deposited on MgO indicates single-crystal, cubic phase ScN; with the (002) and (004) reflections of the ScN film matching the underlying MgO substrate as shown in Fig. 3(c). Given that both ScN and MgO typically crystallize in a cubic rock salt phase ( $Fm\bar{3}m$ ), the ScN is likely grown epitaxially to the underlying MgO substrate giving rise to the shared out-of-plane (001) orientation. Based on the (002) and (004) peak positions of ScN, the out-of-plane lattice constant displays a slight elongation with  $a_0 = 4.54 \text{ \AA}$  as compared to the bulk value of  $a_0 = 4.50 \text{ \AA}$ .<sup>36</sup> This is likely due to the compressive epitaxial strain imposed by the MgO substrate. Phi-scans were performed on the ScN on MgO films which confirmed in-plane orientation, showing the expected 4-fold symmetry due to the shared cubic structure [supplementary material, Fig. S8(b)].

This is the author's peer reviewed, accepted manuscript. However, the online version of record will be different from this version once it has been copyedited and typeset.  
PLEASE CITE THIS ARTICLE AS DOI: 10.1116/6.0004180

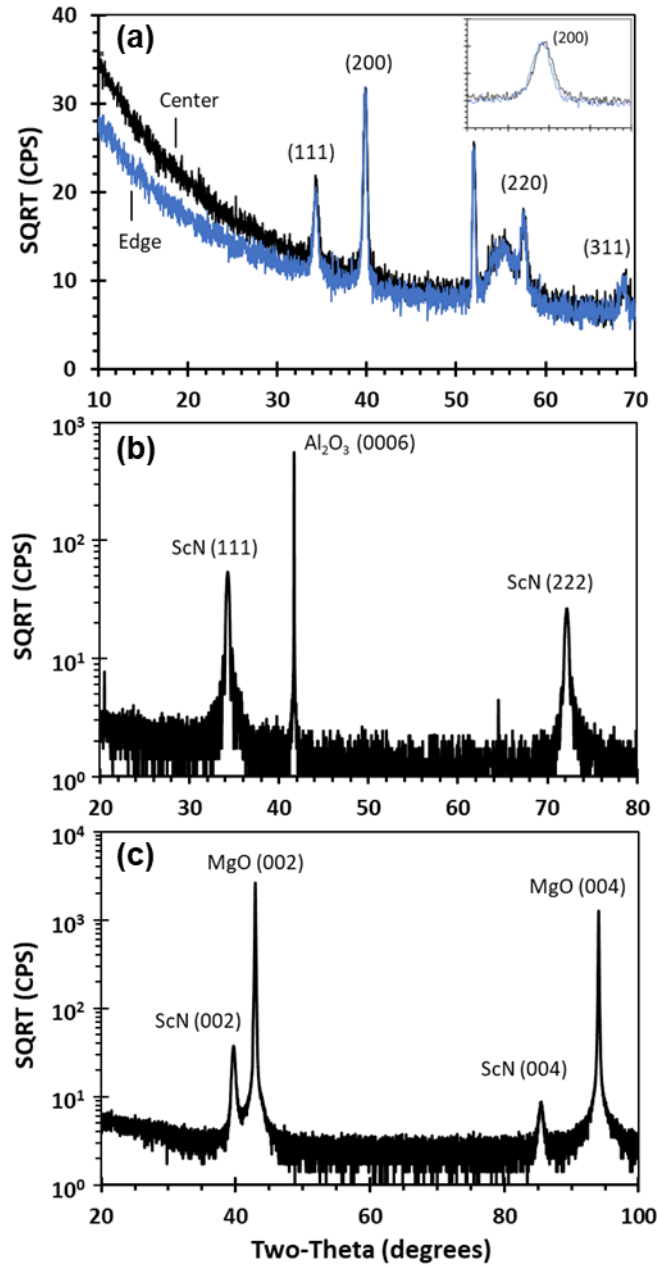


FIG. 3. (a) GIXRD patterns for ScN on 150 mm Si (100) at center and edge positions indicative of a uniform, polycrystalline, cubic structure. XRD patterns for ScN on (b) Al<sub>2</sub>O<sub>3</sub> (0001) and (c) MgO (001) are indicative of single-crystal, cubic phase growth.

FESEM images in Fig. 4 provide (a) top- and (b) cross-sectional views taken from the center position of ScN#2, where columnar grains with sizes ranging from 16–28 nm are observed. Film thickness is estimated at 43 nm, which provides good agreement with the average SE thickness of 41.9 nm reported above. Film conformality was also examined by depositing ScN over 4:1 aspect ratio trench structures shown in Fig. 4(c). These trenches were fabricated by RIE, where the opening measures 312 nm; the corresponding depth is 1.29  $\mu\text{m}$ . The ScN film conformed well to the undulated etched Si surface, achieving a thickness of 36 nm on the top and 27 nm at the bottom of the trenches, resulting in a top-to-bottom thickness ratio of 75% (supplementary material, Fig. S9). Since the mean free path of the gas/vapor species in the reactor is more than two orders-of-magnitude larger than the trench width, the variation in thickness observed in Fig. 4(c) can be attributed to the ballistic transport and reaction kinetics of precursor gases/vapors, particularly plasma species, within the narrow confines of the trench structures. No attempt was made to optimize the ScN PEALD process (such as significantly increasing dose times) for improving coverage across the high aspect ratio (HAR), nm-scale features.

Electrical properties were also evaluated for the ScN films deposited on  $\text{Al}_2\text{O}_3$  (0001) and MgO (001) substrates represented by Fig. 3(b) and Fig. 3(c), respectively. ScN was deposited concurrently on both substrates, along with the HAR substrate shown in Fig. 4(c). A small (~2 cm x 2 cm) Si (100) substrate was also included as a witness sample. Film thickness determined by SE on the Si witness sample was 34.3 nm (index = 2.39), which provides good agreement with the 36 nm ScN thickness measured by FESEM at the top of the HAR trench structures (supplementary material, Fig. S8). ScN film thicknesses on the  $\text{Al}_2\text{O}_3$  (0001) and MgO (001) substrates were 32.5 and 42.0 nm, respectively, as determined by XRR measurements. The increased ScN PEALD film thickness on MgO indicates enhanced nucleation and growth on the underlying MgO (001)



substrate, which shares the same cubic rock salt structure. Hall measurements were subsequently performed to determine the average values for ScN resistivity, mobility and carrier concentration on each substrate. A summary of these results are presented in Table II.

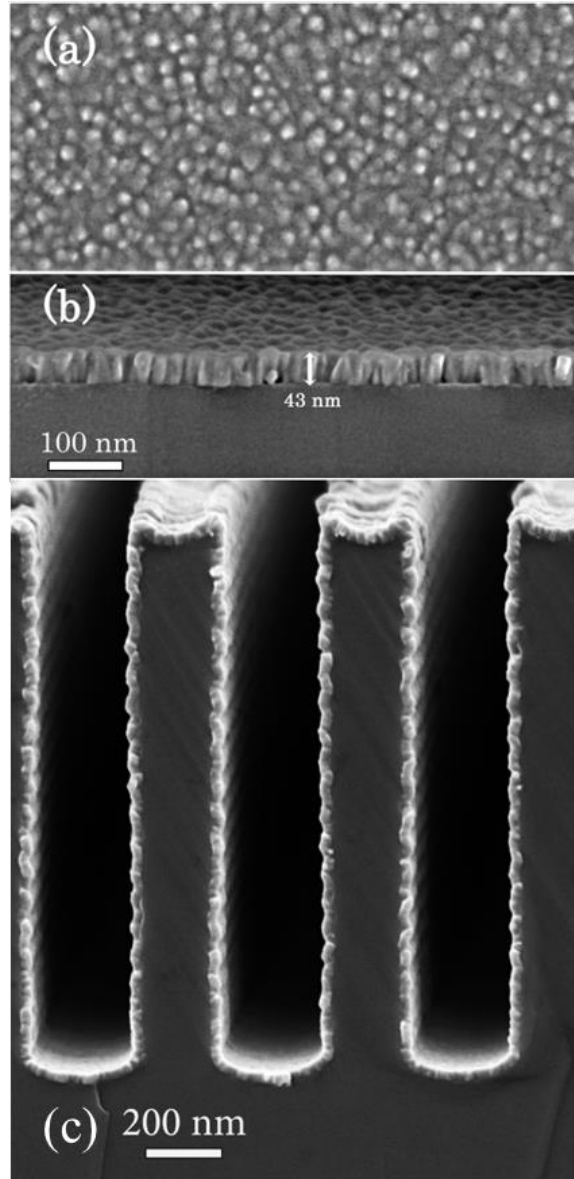


FIG. 4. FESEM images of ScN#2 showing (a) top- and (b) cross-sectional views of the polycrystalline, cubic phase ScN film deposited on Si (100). (c) ScN-coated trenches with a 4:1 aspect ratio imaged by FESEM.

TABLE II. Summary of Hall measurement results for ScN.

<i>Substrate Material</i>	<i>Resistivity (<math>m\Omega\text{-cm}</math>)</i>	<i>Mobility (<math>\text{cm}^2/\text{Vs}</math>)</i>	<i>Carrier Conc. (<math>\text{cm}^{-3}</math>)</i>
Al <sub>2</sub> O <sub>3</sub> (0001)	13.9	23.5	$2.36 \times 10^{19}$
MgO (001)	1.01	298.0	$2.35 \times 10^{19}$

Density functional theory (DFT) calculations by Deng et al., predicted a direct band gap at 2.02 eV for intrinsic cubic phase ScN.<sup>3</sup> High quality ScN epilayers grown by HVPE, with very low levels of impurities, were reported by Oshima et al.,<sup>4</sup> where the direct band gap was measured at 2.06 eV. This measured band gap is in good agreement with the calculated value of 2.02 eV by Deng. Free electron concentrations, however, ranged from  $10^{18}$ – $10^{20}$   $\text{cm}^{-3}$  for nominally undoped ScN films. These carrier concentrations could not be attributed to impurities, but could be related to native point defects (e.g., nitrogen vacancies) in the bulk of the ScN film.<sup>2,7</sup> The results of the study by Deng also showed that for epitaxial layers grown by reactive magnetron sputtering, the direct band gap increased between 2.18–2.7 eV with increasing carrier concentration ranging from  $1.12$ – $12.8 \times 10^{20}$   $\text{cm}^{-3}$ , respectively. The increase in the band gap and free electron concentration were attributed to an increase in fluorine (F) impurities serving as n-type donors, which were unintentionally incorporated into the film due to sputter target contamination. Film composition measured by Auger electron spectroscopy (AES) and XPS determined that F impurity levels ranged from below the AES-XPS detection limit to 3 at.% F. A similar relationship between the direct band gap and carrier concentration was observed by Moram et al., but the increase was attributed to O impurities.<sup>5</sup> In this case, the direct band gap increased between 2.2 and 3.1 eV with

carrier concentrations ranging from  $10^{21}$  and  $10^{22}$   $\text{cm}^{-3}$ , respectively. The effect of F, O, H and tantalum (Ta) impurities on carrier concentration in bulk cubic phase ScN was theoretically investigated by Kumagai et al., which showed that these elements act as either single (O) or double n-type donors (H, F, Ta).<sup>2</sup>

For PEALD ScN, the measured carrier concentrations reported in Table II are significantly lower than the values reported by Deng<sup>3</sup> and Moram<sup>5</sup> described above. However, these values are consistent with those reported by Oshima<sup>4</sup> for high quality ScN epilayers grown by HVPE with very low levels of impurities. For ScN deposited epitaxially on MgO (001) by PEALD, the measured mobility of  $298 \text{ cm}^2/\text{Vs}$  is also consistent with the mobility reported by Oshima at  $284 \text{ cm}^2/\text{Vs}$  for films grown by HVPE on m-plane sapphire. The higher mobility reported here could be due to improved crystalline quality for ScN deposited on MgO (001) vs. m-plane sapphire. For epitaxial ScN deposited on  $\text{Al}_2\text{O}_3$  (0001) by PEALD, the measured mobility of  $23.5 \text{ cm}^2/\text{Vs}$  is in good agreement with reported values ranging from  $1\text{--}30 \text{ cm}^2/\text{Vs}$ .<sup>9,37</sup> More work is needed, however, to better understand the electrical properties of ScN by PEALD techniques.

#### IV. CONCLUSIONS

High purity ScN films by PEALD were grown on Si (100),  $\text{Al}_2\text{O}_3$  (0001) and MgO (001) substrates under UHP conditions. The precursors used were  $\text{ClSc}(\text{EtCp})_2$  and  $\text{N}_2\text{-H}_2$  plasma species at substrate temperatures ranging from  $200\text{--}300^\circ\text{C}$ , where an ALD window was identified between  $200\text{--}215^\circ\text{C}$ . Above this window, pyrolysis of the Sc precursor was observed. For ScN grown at  $215^\circ\text{C}$  on Si (100), XPS depth profiling showed the film was slightly Sc rich containing 48.6 at.% Sc and 47.4 at.% N (N:Sc = 0.97). Impurities were also present in the bulk of the film including 2.5 at.% Cl, 0.9 at.% C and 0.4 at.% O. The oxygen content measured was just above

the detection limit of the XPS instrument. GIXRD measurements produced (111), (200), (220) and (311) reflections matching polycrystalline, cubic phase ScN. For XPS and GIXRD, center and edge positions were measured on 150 mm Si substrates where similar results were obtained, thereby confirming ScN composition and structure across the wafer (elemental concentrations defined above are averages corresponding to the center and edge positions).

FESEM images revealed columnar grains with sizes ranging from 16–28 nm. ScN conformality across 4:1 aspect ratio trench structures was also imaged by FESEM which showed a top-to-bottom thickness ratio of 75%. Out-of-plane x-ray diffraction patterns indicated single-crystal, cubic phase ScN deposited at 215°C on sapphire (0001) and magnesium oxide (001) substrates; phi-scans confirmed epitaxial growth. ScN electrical properties were evaluated by performing Hall measurements to determine mobility, free electron concentration and resistivity. For ScN PEALD on magnesium oxide (001), the average mobility was 298 cm<sup>2</sup>/Vs with a carrier concentration of 2.88 x 10<sup>19</sup> cm<sup>-3</sup>. The average resistivity was 0.822 mΩ·cm.

## ACKNOWLEDGMENTS

The authors would like to thank Nathaniel Nelson of the Kurt J. Lesker Company for his assistance with film analysis, and The Pennsylvania State University Nanofabrication and Materials Characterization Labs for their support of this research. In particular, Guy Lavallee and Michael Labella, III for fabricating the HAR trench structures, as well as Nichole Wonderling and Anthony Richardella for x-ray characterization and data analysis. We would also like to thank Dockweiler Chemicals GmbH for helpful discussions regarding the ClSc(EtCp)<sub>2</sub> precursor and the thermal analysis they provided.

## DATA AVAILABILITY

The data that supports the findings of this study are available within the article [and its supplementary material].

## CONFLICT OF INTEREST

The authors have no conflicts to disclose.

## REFERENCES

- <sup>1</sup>Sai Mu, Andrew J. E. Rowberg, Joshua Leveillee, Feliciano Giustino and Chris G. Van de Walle, Phys. Rev. B **104**, 075118 (2021).
- <sup>2</sup>Yu Kumagai, Naoki Tsunoda and Fumiyasu Oba, Phys. Rev. Appl. **9**, 034019 (2018).
- <sup>3</sup>Ruopeng Deng, B. D. Ozsdolay, P. Y. Zheng, S. V. Khare and D. Gall, Phys. Rev. B **91**, 045104 (2015).
- <sup>4</sup>Yuichi Oshima, Encarnación G. VÍllora and Kiyoshi Shimamura, J. Appl. Phys. **115**, 153508 (2014).
- <sup>5</sup>M. A. Moram, Z. H. Barber and C. J. Humphreys, Thin Solid Films **516** 8569-8572, (2008).
- <sup>6</sup>D. Gall et al., J. Vac. Sci. Technol. A **16**, 2411-2417 (1998).
- <sup>7</sup>Arthur R. Smith, Hamad A. H. AL-Brithen, David C. Ingram, Daniel Gall, J. Appl. Phys. **90**, 1809-1816 (2001).
- <sup>8</sup>Duc V. Dinh, Frank Peiris, Jonas Lähnemann, and Oliver Brandt, Appl. Phys. Lett. **123**, 112102 (2023).
- <sup>9</sup>Sit Kerdsonpanya, Ngo Van Nong, Nini Pryds, Agnė Žukauskaitė, Jens Jensen, Jens Birch, Jun



- Lu, Lars Hultman, Gunilla Wingqvist and Per Eklund, *Appl. Phys. Lett.* **99**, 232113 (2011).
- <sup>10</sup>Bivas Saha, Timothy D Sands and Umesh V Waghmare, *J. Phys.: Condens. Matter* **24**, 415303, (2012).
- <sup>11</sup>Polina V. Burmistrova, Jesse Maassen, Tela Favaloro, Bivas Saha, Shuaib Salamat, Yee Rui Koh, Mark S. Lundstrom, Ali Shakouri and Timothy D. Sands, *J. Appl. Phys.* **113**, 153704 (2013).
- <sup>12</sup>Jeremy L. Schroeder, David A. Ewoldt, Reja Amatya, Rajeev J. Ram, Ali Shakouri and Timothy D. Sands, *J. Microelectromech. S.* **23**, 672-680 (2014).
- <sup>13</sup>Sit Kerdsongpanya, Olle Hellman, Bo Sun, Yee Kan Koh, Jun Lu, Ngo Van Nong, Sergei I. Simak, Björn Alling and Per Eklund, *Phys. Rev. B* **96**, 195417 (2017).
- <sup>14</sup>Dheemahi Rao, Bidesh Biswas, Eduardo Flores, Abhijit Chatterjee, Magnus Garbrecht, Yee Rui Koh, Vijay Bhatia, Ashalatha Indiradevi Kamalasanan Pillai, Patrick E. Hopkins, Marisol Martin-Gonzalez and Bivas Saha, *Appl. Phys. Lett.* **116**, 152103 (2020).
- <sup>15</sup>M. J. Kappers, M. A. Moram, Y. Zhang, M. E. Vickers, Z. H. Barber and C. J. Humphreys, *Physica B* **401-402**, 296–301 (2007).
- <sup>16</sup>C. F. Johnston, M. J. Kappers, M. A. Moram, J. L. Hollander and C. J. Humphreys, *J. Cryst. Growth* **311**, 3295-3299 (2009).
- <sup>17</sup>M. A. Moram, M. J. Kappers and C. J. Humphreys, *Phys. Status Solidi C* **7**, 1778-1780 (2010).
- <sup>18</sup>Morito Akiyama, Toshihiro Kamohara, Kazuhiko Kano, Akihiko Teshigahara, Yukihiro Takeuchi, and Nobuaki Kawahara, *Adv. Mater.* **21**, 593-596 (2009).
- <sup>19</sup>Simon Fichtner, Niklas Wolff, Fabian Lofink, Lorenz Kienle, and Bernhard Wagner, *J. Appl. Phys.* **125**, 114103 (2019).
- <sup>20</sup>Olaf Zywitzki, Thomas Modes, Stephan Barth, Hagen Bartzsch, Peter Frach, *Surf. Coat. Tech.*



- 309**, 2017, 417-422 (2017).
- <sup>21</sup>Marc-Alexandre Dubois and Paul Muralt, *Appl. Phys. Lett.* **74**, 3032–3034 (1999).
- <sup>22</sup>R. Ruby and P. Merchant, *Proceedings of IEEE 48<sup>th</sup> Annual Symposium on Frequency Control* (Boston, MA, USA, 1994), pp. 135-138.
- <sup>23</sup>Milena Moreira, Johan Bjurström, Ilia Katardjev, Ventsislav Yantchev, *Vacuum* **86**, 23-26 (2011).
- <sup>24</sup>Tom-Niklas Kreutzer, Simon Fichtner, Bernhard Wagner and Fabian Lofink, *IEEE International Symposium on Applications of Ferroelectrics* (Sydney, Australia, 2021), pp. 1-3.
- <sup>25</sup>Qi Wang, Yipeng Lu, Sergey Mishin, Yury Oshmyansky and David A. Horsley, *J. Microelectromech. S.* **26**, 1132-1139 (2017).
- <sup>26</sup>Dixiong Wang, Jeffrey Zheng, Pariasadat Musavigharavi, Wanlin Zhu, Alexandre C. Foucher, Susan E. Troler-McKinstry, Eric A. Stach and Roy H. Olsson III, *IEEE Electr. Device L.* **41**, 1774-1777 (2020).
- <sup>27</sup>Daniel Drury, Keisuke Yazawa, Andriy Zakutayev, Brendan Hanrahan and Geoff Brennecke, *Micromachines-Basel* **13**, 887 (2022).
- <sup>28</sup>Maryam S. Hosseini, Masoumeh Ebrahimi, Pooria Yaghini and Nader Bagherzadeh, *IEEE Transactions on Emerging Topics in Computing* **10**, 1657-1664 (2022).
- <sup>29</sup>Nicholas A. Strnad, Daniel M. Potrepka, Brendan M. Hanrahan, Glen R. Fox, Ronald G. Polcawich, Jeffrey S. Pulskamp, Ryan R. Knight and Ryan Q. Rudy, *J. Vac. Sci. Technol. A* **41**, 050801 (2023).
- <sup>30</sup>Tai Nguyen, Nouredine Adjeroud, Sebastjan Glinsek, Yves Fleming, Jérôme Guillot, Patrick Grysan and Jérôme Polesel-Maris, *APL Mater.* **8**, 071101 (2020).



- <sup>31</sup>Elmeri Österlund, Heli Seppänen, Kristina Bespalova, Ville Miikkulainen, and Mervi Paulasto-Kröckel, *J. Vac. Sci. Technol. A* **39**, 032403 (2021).
- <sup>32</sup>N. A. Strnad et al, *J. Vac. Sci. Technol. A* **40**, 042403 (2022).
- <sup>33</sup>A. Shih, J. E. Yater, C. Hor, R. Abrams, *Applied Surface Science* **211**, 136-145 (2003).
- <sup>34</sup>Gilbert B. Rayner, Jr., Noel O'Toole, Jeffrey Shallenberger and Blaine Johs, *J. Vac. Sci. Technol. A* **38**, 062408 (2020).
- <sup>35</sup>Rainer Niewa, Dmitry A. Zherebtsov, Martin Kirchner, Marcus Schmidt and Walter Schnelle, *Chem. Mater.* **16**, 5445-5451 (2004).
- <sup>36</sup>Z. Gu, J.H. Edgar, J. Pomeroy, M. Kuball, and D.W. Coffey, *Journal of Materials Science: Materials in Electronics*, **15**, 555-559 (2004).
- <sup>37</sup>T. D. Moustakas, R. J. Molnar and J. P. Dismukes, *Proceedings of the First Symposium on III-V Nitride Materials and Processes*, edited by T. D. Moustakas, J. P. Dismukes and S. J. Pearton (The Electrochemical Society, Inc., Pennington, NJ, USA, 1996), Vol. 96-11, pp. 197-204.